

## PROPER MOTIONS OF H<sub>2</sub>O MASERS IN THE WATER FOUNTAIN SOURCE IRAS 19190+1102

F. M. DAY AND Y. M. PIHLSTRÖM<sup>1</sup>

Department of Physics and Astronomy, University of New Mexico, 800 Yale Blvd NE, Albuquerque, NM 87131

M. J. CLAUSSEN

National Radio Astronomy Observatory (NRAO), Array Operations Center, P.O. Box O, Socorro, NM 87801, USA

AND

R. SAHAI

Jet Propulsion Laboratory, MS183-900, California Institute of Technology, Pasadena, CA 91109, USA

*Draft version October 29, 2018*

### ABSTRACT

We report on the results of two epochs of Very Long Baseline Array (VLBA) observations of the 22 GHz water masers toward IRAS 19190+1102. The water maser emission from this object shows two main arc-shaped formations perpendicular to their NE-SW separation axis. The arcs are separated by  $\sim 280$  mas in position, and are expanding outwards at an angular rate of  $2.35$  mas yr<sup>-1</sup>. We detect maser emission at velocities between  $-53.3$  km s<sup>-1</sup> to  $+78.0$  km s<sup>-1</sup> and there is a distinct velocity pattern where the NE masers are blueshifted and the SW masers are redshifted. The outflow has a three-dimensional outflow velocity of  $99.8$  km s<sup>-1</sup> and a dynamical age of about 59 yr. A group of blueshifted masers not located along the arcs shows a change in velocity of more than  $25$  km s<sup>-1</sup> between epochs, and may be indicative of the formation of a new lobe. These observations show that IRAS 19190+1102 is a member of the class of “water fountain” pre-planetary nebulae displaying bipolar structure.

*Subject headings:* masers – stars: mass loss

### 1. INTRODUCTION

Intermediate mass stars ( $1-8 M_{\odot}$ ) evolve from being asymptotic giant branch (AGB) stars into planetary nebulae (PNs) via a short transition phase during which the stars are classified as pre-planetary nebulae (PPNs). AGB stars lose mass from a slow, dense wind with expansion velocities of  $5-30$  km s<sup>-1</sup> and exhibit roughly spherically symmetric circumstellar shells; however, PNs are often observed to have aspherical morphologies, including multipolar and elliptical structures (e.g., Sahai & Trauger 1998; Sahai et al. 2000b; Sahai et al. 2007). Presumably it is during the PPN stage that some mechanism, responsible for the shaping of the wide variety of PN morphologies, becomes operational. Due to the short lifetime of PPNs, few objects have been studied during this specific stage and the details of the evolution of an AGB star into a PN still remain unclear.

Understanding the short PPN stage is fundamental for understanding the final stages of intermediate mass stellar evolution. As PPNs exhibit bipolar outflows (e.g., Sahai et al. 2007), it is now believed that jets are important in shaping multipolar PNs (Sahai & Trauger 1998). Detailed observations of individual objects can provide information about the prevailing physical conditions under which the PN morphologies are formed, and about the progenitor star. To study the effects of jets in these objects, kinematical information concerning the outflows is crucial. Radio H<sub>2</sub>O, OH, and SiO

maser line emission can be used to aid classification of these objects in their late stages of evolution. In “water fountain” nebulae, high-velocity H<sub>2</sub>O masers (velocity spreads  $> 50$  km s<sup>-1</sup>) are believed to trace high-velocity outflows. Such high-velocity water masers were first discovered in IRAS 16342-3814 (Likkell & Morris 1988), and several more water fountain PPN candidates have been discovered via their single dish spectra. High angular resolution observations of water masers in IRAS 16342-3814, OH 12.8-0.9, IRAS 19134+2131, W43A, and IRAS 16552-3040 (Claussen et al. 2009; Boboltz & Marvel 2007; Imai et al. 2007; Suárez et al. 2008) have confirmed their classification as water fountains, by showing a spatial and kinematical structure consistent with bipolar lobes. Individual maser features persist on 1–3 year periods (Engels 2002) and can thus be used to trace dynamics of the gas.

Accurate distance measures to PPNs as well as PNs in our galaxy are sparse, thus limiting the accuracy of derived stellar properties. Observations using the VLBA allow high precision ( $< 1$  mas at 22 GHz) astrometric studies of the maser features in PPNs, therefore enabling the possibility of performing trigonometric parallax measurements. The measured proper motions of the masers is a combination of three components: motion of the gas relative to the central object, peculiar motion of the source within the galaxy, and parallax. By measuring these motions we can determine distances to and dynamical ages of PPNs, thereby affording further understanding of the transition from the AGB to PN phase, including luminosity, mass, and mass loss rate.

IRAS 19190+1102 is an OH and H<sub>2</sub>O source with *In-*

fonda@unm.edu

<sup>1</sup> Y. M. Pihlström is also an Adjunct Astronomer at the National Radio Astronomy Observatory.

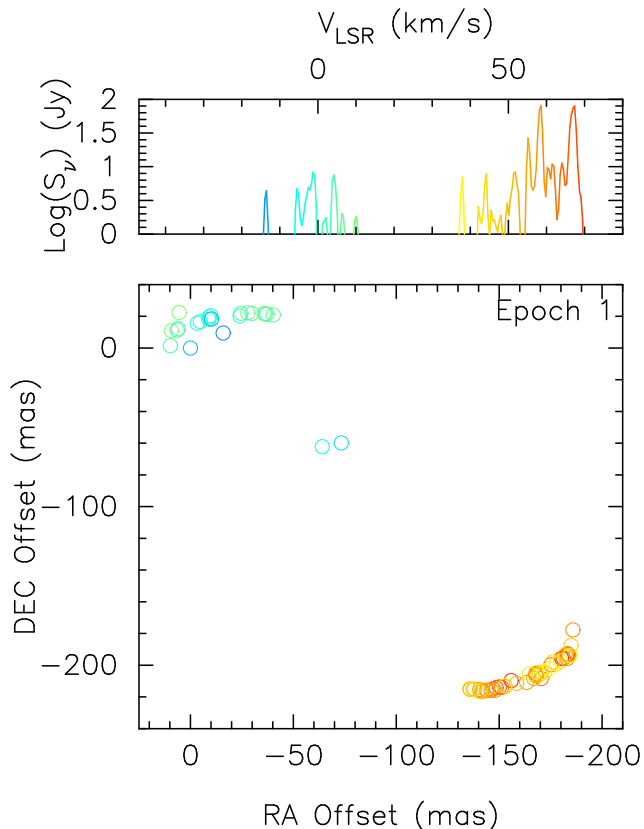


FIG. 1.— 2004 March 19 (Epoch 1) Top panel: log plot of the spectral distribution of maser emission in IRAS 19190+1102. Bottom panel: spatial distribution of masers in IRAS 19190+1102, relative to the feature at (0,0).

frared Astronomical Satellite (IRAS) colors characteristic of evolved stars ( $[25-60] \lesssim 1.5$  and  $[12-25] \gtrsim 1.4$ , where  $[a-b] = 2.5 \log(S_b/S_a)$ ). Likkel (1989) first observed the OH & H<sub>2</sub>O emission in this source, finding the velocity range of the H<sub>2</sub>O emission spanned more than 70 km s<sup>-1</sup>, atypical of OH/IR stars. In this paper, we present high spatial resolution data identifying IRAS 19190+1102 as a water fountain PPN. We give initial results (two epochs) of observations of H<sub>2</sub>O maser emission from IRAS 19190+1102, as well as a brief discussion of its far-infrared characteristics, and discuss its classification as a water fountain PPN. This source is our first target to which we will perform parallax measurements on (to be presented in a subsequent paper).

## 2. OBSERVATIONS AND DATA REDUCTION

VLBA spectral line observations of IRAS 19190+1102 were taken 2004 March 19 and 2006 May 31 of the 22.235 GHz  $6_{16} \rightarrow 5_{23}$  H<sub>2</sub>O transition. Observations were made using a 16 MHz band with dual circular polarization, consisting of 1024 channels centered around  $V_{\text{LSR}} = 50$  km s<sup>-1</sup>. Thus the velocity coverage was -58 to +157 km s<sup>-1</sup> with a spectral resolution of 0.21 km s<sup>-1</sup> per channel. Total on-source time for each observation was  $\sim 3.5$  hr. The data were correlated at the VLBA correlator in Socorro, NM.

The AIPS package was used to reduce and analyze the data. The bandpass response and residual delays were determined using the source 3C454.3. For these observations phase-referencing was not used so global fitting

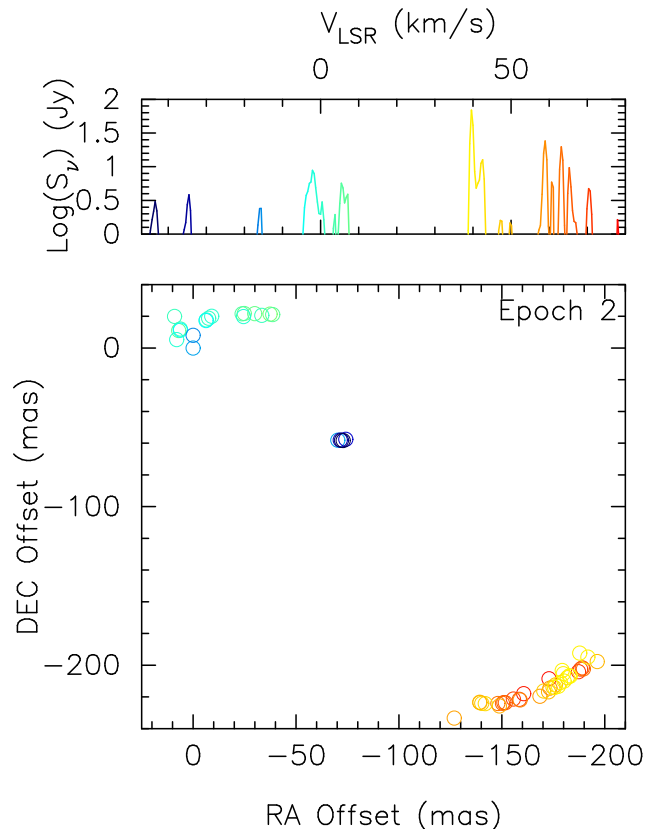


FIG. 2.— 2006 May 31 (Epoch 2) Top panel: log plot of the spectral distribution of maser emission in IRAS 19190+1102. Bottom panel: spatial distribution of masers in IRAS 19190+1102, relative to the feature at (0,0).

of the fringe rates were obtained by fringe fitting on a maser feature identified in both epochs. Furthermore, an iterative self-calibration and imaging procedure was used to improve the SNR, hence absolute positions of the phase centers was lost. Three of the ten antennas were flagged in both epochs due to poor SNR, and each epoch was imaged with a beam size of  $1.58 \text{ mas} \times 0.96 \text{ mas}$ . The spectra were averaged to a velocity resolution of 0.42 km s<sup>-1</sup> per channel to improve the SNR for weaker masers. Final cubes of both epochs had an rms of  $\sigma \sim 10$  mJy per channel for channels without line emission; rms noise in channels containing the brightest emission were found to be  $\sigma = 20$  mJy, 40 mJy for the first and second epochs, respectively.

For a detection to be considered significant, emission had to span more than one 0.42 km s<sup>-1</sup> wide channel, and a cutoff flux density was set at 10 times the rms noise of each channel. We obtained maser component parameters by fitting two-dimensional Gaussian functions to emission in individual channels. Maser emission was spread over more than one channel, so we used a flux-density-squared, weighted-averaging scheme to calculate each maser feature's central velocity and position. Errors from using the weighted-average were less than the velocity resolution, and less than 0.5 mas in position.

Because we were unable to obtain absolute positions of the maser features, we measured relative positions with respect to a feature being common in both epochs. Although this feature drifted in velocity by almost 2 km s<sup>-1</sup> between the two epochs (indicating that perhaps some

acceleration may be present which could be investigated with future epochs), its relative position with respect to several nearby masers is persistent and we therefore identify this maser as being the same in both epochs. Moreover, a test using a different reference maser did not change the results reported on in this paper. Table 1 (epoch 1) and Table 2 (epoch 2) include maser velocity, flux and its associated error, relative right ascension and its associated error, and relative declination and its error. The flux assigned to a maser feature was the peak flux in the channels the feature spanned.

### 3. RESULTS

The spatial distribution of maser emission in both epochs shows two main arc-shaped formations, arranged perpendicular to a NE-SW separation axis ( $\sim 34$  degrees east of north). Spectral and spatial distributions of the  $\text{H}_2\text{O}$  masers are shown in Figures 1 (epoch 1) and 2 (epoch 2). Log plots were used to show the spectral distribution of the maser features in order to show more detail of the weaker, blueshifted features. The northern features are blueshifted ( $-17.9$  to  $11.4$   $\text{km s}^{-1}$ ), and southern features are redshifted ( $28.8$  to  $78.0$   $\text{km s}^{-1}$ ). Furthermore, both epochs have a third group of masers, which are not located within the arc-like structures, but instead appear along the axis of separation (see section 4.3). The total velocity spread of the masers is  $\Delta V \sim 90$   $\text{km s}^{-1}$  in epoch 1 and  $\Delta V \sim 130$   $\text{km s}^{-1}$  in epoch 2.

The arcs in epoch 1 are  $53.65$  mas (northern arc) and  $62.44$  mas (southern arc) across, whereas the arcs were only measured to be  $49.23$  mas (northern arc) and  $62.62$  mas (southern arc) across in epoch 2. Even though the rms noise is slightly higher in the second epoch for the channels with bright emission, the masers in the edges of the arcs appear to have on average the same flux density as masers closer to the center and so we should have been able to detect these masers. Therefore it appears as if the physical extent of conditions for masers to occur has decreased somewhat for the northern arc in the second epoch. The average angular separation of the north and south masers is  $269.27 \pm 0.24$  mas in epoch 1 and  $279.60 \pm 0.30$  mas in epoch 2. Using  $d = 8.6$  kpc as the distance to IRAS 19190+1102 (see section 4.2), the separation of the arcs is then  $2316$  AU and  $2405$  AU for epochs 1 and 2, respectively.

Since maser emission can be variable in both flux and velocity, and due to the large number of detections in each cube, it is difficult to analyze the kinematics of individual maser features. Instead, we used the average angular separation to measure maser proper motions. We assume that the northern and southern arcs are expanding at equal rates, and so we halve the difference in angular separation to get an expansion rate of  $\mu = 2.35 \pm 0.18$  mas  $\text{yr}^{-1}$ . The age for the jet, then, is estimated to be  $\sim 59$  yr, assuming that the proper motion is constant. The average line of sight velocity of the the  $\text{H}_2\text{O}$  masers is  $V_r = 27.6$   $\text{km s}^{-1}$ , which, when combined with the tangential speed of the masers ( $V_t = \mu d = 95.9$   $\text{km s}^{-1}$ ), yields a total 3D outflow speed,  $V_{exp} = \sqrt{V_r^2 + V_t^2}$ , of  $99.8$   $\text{km s}^{-1}$ . The inclination angle with respect to the plane of the sky was calculated to be  $i = \tan^{-1}(V_r/V_t) = 16.1^\circ$ . By assuming that the dynamical center of the outflow is located at the midpoint along the axis of separation of

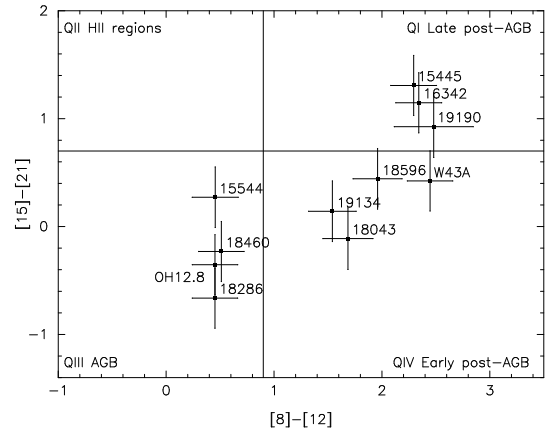


FIG. 3.— *MSX* color-color diagram showing locations of known and candidate water fountain sources within the quadrants defined by Sevenster (2002). The location of IRAS 19190+1102 strongly supports the conclusion that it truly is an evolved object, as opposed to a star forming region.

the arc-like structures, we obtain jet opening angles of  $\phi_1 \sim 11^\circ - 13^\circ$  for epoch 1 and  $\phi_2 \sim 10^\circ - 13^\circ$  for epoch 2.

## 4. DISCUSSION

### 4.1. A True Water Fountain PPN

In order for an object to be classified as a true water fountain PPN, it needs to display both water maser fountain characteristics as well as being an evolved star. Likkell (1989) detected OH 1612, 1667 and  $\text{H}_2\text{O}$  masers in IRAS 19190+1102, but due to the OH and  $\text{H}_2\text{O}$  features' peculiar nature (e.g. a third peak in the 1612 MHz emission,  $\text{H}_2\text{O}$  emission spanning more than  $70$   $\text{km s}^{-1}$ ) and cold *IRAS* colors, it was not definitively classified as an evolved star at that time. In *IRAS* color-color (e.g.  $[25-60]$  vs  $[12-25]$ ) diagrams, there is some overlap in the regions occupied by HII regions, young stellar objects (YSOs), evolved stars and PNs. Furthermore, Mottram et al. (2007) include IRAS 19190+1102 (G046.2561-01.4763) as a candidate massive YSO based on its mid-infrared colors. However, combining spectral properties of e.g. OH and  $\text{H}_2\text{O}$  with *IRAS* and *Midcourse Space eXperiment (MSX)* colors can help distinguish evolved stars from very young objects (c.f. Sevenster 2002).

The location of IRAS 19190+1102 in the *IRAS* color-color diagram places it in the post-AGB region, and its *MSX* fluxes tentatively place it in quadrant I (late post-AGB region) as defined by Sevenster (2002). Figure 3 is a modification of the *MSX* color-color diagram of known and candidate water fountain sources made by Suárez et al. (2008), with IRAS 19190+1102 included as well as each source's three sigma error bars. Although the  $8\mu\text{m}$  and  $12\mu\text{m}$  fluxes are at the limit of detection (*MSX* quality flag 1, with  $\text{SNR} \approx 4.5$  in both bands), the position of IRAS 19190+1102 lies well within the quadrant containing post-AGB objects. Moreover, the 1612 MHz OH emission is stronger than the 1667 MHz OH emission (Likkell 1989) which is also consistent with what is observed in the thick circumstellar shells of evolved OH/IR stars. Thus we postulate that IRAS 19190+1102 truly is an evolved object. Our VLBA observations confirm that the bipolar structure, outward expansion, and high-velocity  $\text{H}_2\text{O}$  masers of IRAS 19190+1102 make it a water fountain PPN.

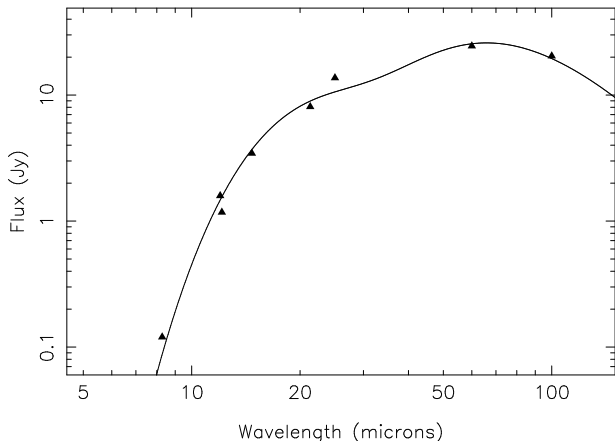


FIG. 4.— The far-infrared emission observed from IRAS 19190+1102. Also shown is the calculated flux (continuous line) with dust emissivity  $\propto \nu^{1.5}$  for a particular best-fit model. At least two different dust components, with different temperatures and masses, are required to fit the data.

#### 4.2. Molecular Gas and Dust

The infrared emission in IRAS 19190+1102 can be used as an estimate of the dust mass, and its temperature (Sahai et al. 1991). Using the *IRAS* fluxes of IRAS 19190+1102 (1.59, 13.67, 24.52, and 20.41 Jy in the 12, 25, 60 and 100 $\mu$  bands) as well as its *MSX* fluxes (0.12017, 1.17535, 3.4499, and 8.0921 Jy in the 8, 12, 15, and 21 $\mu$  bands), we find that two dust components with temperatures of 46 K and 120 K are required to fit the data according to the model described in Sahai et al. (1991). The masses of the two dust components are, respectively,  $M_{dust} = 0.7 \times 10^{-3}(d/1 \text{ kpc})^2 M_{\odot}$  and  $0.4 \times 10^{-5}(d/1 \text{ kpc})^2 M_{\odot}$ . Figure 4 shows the results of the fit of the data with a peak of the spectral energy distribution (SED) between 60 and 100 $\mu$ m.

The distance to IRAS 19190+1102 is poorly known, and has been quoted as low as 1.5 kpc (Preite-Martinez 1988). Preite-Martinez (1988) used the modified Shklovsky method to determine the distance to IRAS 19190+1102, whereby the ionized mass of a PN is related to its electron density. However, Van de Steene & Pottasch (1995) did not detect 6-cm continuum emission in IRAS 19190+1102 down to 3 to 4 mJy, so most of its nebular mass is not ionized, making a distance of 1.5 kpc suspect. We instead estimate the distance assuming that IRAS 19190+1102 has a typical PPN luminosity of 6000  $L_{\odot}$  (Sahai et al. 2007), in which case it can be placed as far away as  $d = 8.6$  kpc using our SED fit of the far-infrared fluxes. In this paper we therefore adopted a distance to IRAS 19190+1102 of 8.6 kpc.

Furthermore, by assuming a distance of  $d = 8.6$  kpc and a typical gas-to-dust ratio of 200, the total dust mass of IRAS 19190+1102 is  $0.05 M_{\odot}$  and the total gas mass is close to  $10 M_{\odot}$ . The mass estimate is, of course, very uncertain; the largest uncertainty is due to the mass derivation's square dependence on distance, followed by uncertainties in the dust mass derivation and gas-to-dust ratio. Hence our estimate of  $10 M_{\odot}$  is not necessarily inconsistent with IRAS 19190+1102 being a PPN. We merely emphasize that the mass for this object is likely to be large—in the upper end of the PPN progenitor stel-

lar mass range.

#### 4.3. Comparisons to Other Water Fountain Sources

There exist at least five other known water fountain sources: IRAS 16342-3814, OH 12.8-0.9, IRAS 19134+2131, W43A, and IRAS 16552-3050 (Claussen et al. 2009; Boboltz & Marvel 2007; Imai et al. 2007; Suárez et al. 2008) as well as numerous other candidates (cf. Imai 2007 and references therein). The age we measure for IRAS 19190+1102 of  $\sim 59$  years is similar to ages of other water fountain nebulae, which lie in the range of 35–130 years. The linear separation of the arcs in IRAS 19190+1102 of 2405 AU at 8.6 kpc places it within the range for other water fountain objects (880 AU for OH 12.8-0.9 up to 6000 AU for IRAS 16342-3814). Our detection of highly collimated outflows ( $\phi \sim 10^{\circ}$ – $13^{\circ}$ ) in this source is characteristic of the other water fountain pre-planetary nebulae, which have  $\phi < 15^{\circ}$  (with the exception of IRAS 16552-3050, in which the opening angle of the outflow is rather large,  $70^{\circ}$  (Suárez et al. 2008)).

As in the case of IRAS 16342-3814, there is no apparent systematic change in velocity along the arcs and there is a group of blue-shifted masers not distributed along the arcs (epoch 1:  $-11$  to  $-8$  km s $^{-1}$ ; epoch 2:  $-16.1$  to  $-53.3$  km s $^{-1}$ ; see Figure 5). Interestingly, in contrast to IRAS 16342-3814, the most blueshifted features in IRAS 19190+1102 in epoch 2 correspond to the group not along the arcs, but are located close to the dynamical center, at a radial distance of about 335–385 AU from the latter. Although this location depends on the unknown distance, it seems unlikely that these masers could be remnants from the AGB OH/IR phase, where H $_2$ O masers occur between 10–100 AU from the star.

The average velocity of the masers in this central region has changed by more than 25 km s $^{-1}$  between epochs 1 and 2. More observations are necessary to understand their exact nature, and we can just speculate that the masers were created from an episodic or precessing jet hitting new material. Perhaps the dramatic change in velocities of these features could be a result of a new jet hitting clumps with different densities and accelerating them to different speeds. It is also possible that this jet outflow has just started operating and consequently has not reached a steady state like the bipolar jet responsible for creating the slowly expanding arc-like structures. These features may indicate the earliest stages of the formation of a new lobe, and so it is possible that IRAS 19190+1102 will eventually develop minor lobes (c.f. the PPNs Frosty Leo (Sahai et al. 2000a) and AFGL 2688 (Sahai et al. 1998)) or become a multipolar nebula (c.f. IRAS 19475+3119, IRAS 19024+0044 (Sahai et al. 2007)). Thus, monitoring the H $_2$ O masers in IRAS 19190+1102 should be given high priority in future observational studies of water fountain pre-planetary nebulae, for understanding the earliest stages of the formation of bipolar and possibly multipolar structure in these objects.

## 5. CONCLUSIONS

Using the VLBA, we have observed the H $_2$ O masers toward IRAS 19190+1102 with very high angular resolution; these observations indicate that the high-velocity masers span a velocity range  $\Delta V > 130$  km s $^{-1}$  and lie

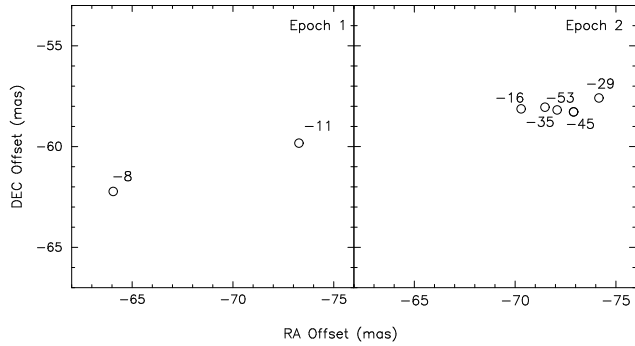


FIG. 5.— A zoom in of the centrally located masers in epoch 1 (left) and epoch 2 (right). The numbers represent the LSR velocity of each maser. The masers in epoch 2 have no counterpart to those in epoch 1, and their velocities are also much different, suggesting they may be the signposts of a new lobe structure which is in an early, unstable formation phase.

in a bipolar structure. The afore mentioned properties indicate that IRAS 19190+1102 is one of six known “water fountain” sources, i.e. very young pre-planetary nebulae in which the presence of collimated, high-velocity outflows is manifest. The arclike structures appear to lie perpendicular to a NE-SW axis, with the blueshifted features to the north and redshifted features to the south. The arclike distributions are suggestive of bow shocks

produced by a collimated jet colliding with surrounding material. The proper motions of the H<sub>2</sub>O masers suggest that the dynamical age of the jet is  $\sim 59$  yr. Additionally, a group of blueshifted masers not located along the arcs was detected in both epochs. These “central” masers showed a dramatic change ( $>25$  km s<sup>-1</sup>) in velocity, which we suggest may signal the beginning of a new lobe due to an episodic or precessing jet.

We have obtained five additional epochs of IRAS 19190+1102 using the VLBA, using the 22 GHz line of H<sub>2</sub>O and the 1612, 1665, 1667, 1720 MHz OH lines. With these observations we anticipate establishing an accurate estimate to the distance of IRAS 19190+1102 via parallax measurements, and thus more precise estimates of its stellar properties.

The National Radio Astronomy Observatory is a facility of the National Science Foundation operated under cooperative agreement by Associated Universities, Inc. RS thanks NASA for partially funding this work via LTSA award (# NM0710651/399-20-40-06), ADP award (# NM0710651/399-20-00-08) and HST/GO award (# GO-09801.01-A).

*Facilities:* VLBA

#### REFERENCES

- Boboltz, D.A., & Marvel, K.B. 2007, ApJ, 665, 680  
 Claussen, M.J., Sahai, R., & Morris, M.R. 2009, ApJ, 29, 219  
 Engels, D. 2002, A&A, 388, 252  
 Imai, H., Sahai, R., & Morris, M. 2007, ApJ, 669, 424  
 Imai, H. 2007, in IAU Symp. 242, Astrophysical Masers and Their Environments, ed. W. Baan & J. Chapman (Cambridge: Cambridge Univ. Press), 279  
 Likkell, L. 1989, ApJ, 344, 350  
 Likkell, L., & Morris, M. 1988, ApJ, 329, 914  
 Mottram, J.C., Hoare, M.G., Lumsden, S.L., Oudmaijer, R.D., Urquhart, J.S., Sheret, T.L., Clarke, A.J., & Allsopp, J. 2007, A&A, 476, 1019  
 Preite-Martinez, A. 1988, A&A, 76, 317  
 Sahai, R., Bujarrabal, V., Castro-Carrizo, A., & Zijlstra, A. 2000a, A&A, 360, L9  
 Sahai, R., Morris, M., Sánchez Contreras, C., & Claussen, M. 2007, AJ, 134, 2200  
 Sahai, R., Su, K.Y.L., Kwok, S., Dayal, A., & Hrivnak, B.J. 2000b, in ASP Conf. Ser. 199, Asymmetrical Planetary Nebulae II: From Origins to Microstructures, ed. J.H. Kastner, N. Soker, & S. Rappaport (San Francisco: ASP), 167  
 Sahai, R., Wootten, A., Schwarz, H.E., & Clegg, R.E.S. 1991, A&A, 251, 560  
 Sahai, R., & Trauger, J.T. 1998, AJ, 116, 1357  
 Sahai, R., Trauger, J.T., Watson, A.M., et al. 1998, ApJ, 493, 301  
 Sevenster, M.N. 2002, AJ, 123, 2772  
 Suárez, O., Gómez, J.F., & Miranda, L.F. 2008, ApJ, 689, 430  
 Van de Steene, G.C., & Pottasch, S.R. 1995, A&A, 299, 238

TABLE 1  
 MASER FEATURES IN EPOCH 1 (2004 MARCH 19). POSITIONS ARE RELATIVE TO THE FEATURE WITH POSITION (0,0) (IN BOLDFACE).

Blueshifted Masers							Redshifted Masers						
$v_{LSR}$ km/s	$S_\nu$ Jy/beam	$\sigma_{S_\nu}$ Jy/beam	$\Delta RA$ mas	$\sigma_{RA}$ mas	$\Delta DEC$ mas	$\sigma_{DEC}$ mas	$v_{LSR}$ km/s	$S_\nu$ Jy/beam	$\sigma_{S_\nu}$ Jy/beam	$\Delta RA$ mas	$\sigma_{RA}$ mas	$\Delta DEC$ mas	$\sigma_{DEC}$ mas
-17.30	0.269	0.008	-15.878	0.021	9.522	0.010	28.77	0.306	0.008	-164.606	0.015	-205.541	0.004
-14.00	0.721	0.008	-10.208	0.012	18.288	0.020	37.83	5.430	0.012	-174.451	0.016	-202.325	0.012
<b>-13.54</b>	<b>4.161</b>	<b>0.007</b>	<b>0.000</b>	<b>0.018</b>	<b>0.000</b>	<b>0.024</b>	37.84	1.214	0.012	-152.751	0.007	-212.977	0.032
-10.68	0.534	0.008	-73.276	0.003	-59.827	0.008	40.59	0.231	0.008	-172.031	0.070	-204.633	0.132
-8.18	0.439	0.007	-64.060	0.009	-62.226	0.005	41.27	0.370	0.008	-184.379	0.011	-193.792	0.028
-7.56	0.369	0.008	-9.003	0.028	18.070	0.123	42.14	2.440	0.009	-179.817	0.002	-197.305	0.017
-5.44	0.813	0.010	-4.817	0.030	16.683	0.017	42.72	0.632	0.009	-137.225	0.199	-215.326	0.029
-5.38	3.674	0.010	-9.117	0.013	19.600	0.018	43.05	0.454	0.009	-177.804	0.071	-198.968	0.068
-2.09	3.076	0.010	-24.094	0.258	20.225	0.178	44.07	7.074	0.013	-175.714	0.064	-199.634	0.054
-2.06	1.105	0.010	-9.897	0.210	20.453	0.082	45.50	1.678	0.009	-140.549	0.039	-216.692	0.009
1.32	1.050	0.009	5.869	0.140	12.163	0.103	45.56	0.732	0.009	-175.942	0.018	-197.951	0.004
1.97	0.625	0.009	9.788	0.015	1.404	0.024	46.41	0.470	0.009	-169.639	0.023	-205.574	0.022
2.34	0.763	0.009	6.391	0.028	11.207	0.099	47.05	0.244	0.009	-184.880	0.003	-187.510	0.035
3.74	0.658	0.010	-37.198	0.015	21.376	0.011	47.95	0.631	0.009	-170.399	0.062	-204.368	0.089
4.17	5.537	0.011	-24.565	0.215	21.907	0.058	48.11	0.484	0.009	-181.991	0.096	-193.642	0.085
4.84	0.244	0.009	-40.205	0.065	20.878	0.015	48.83	2.220	0.009	-135.934	0.403	-215.366	0.168
5.24	0.148	0.008	-35.861	0.065	21.729	0.019	51.30	2.189	0.011	-168.293	0.033	-206.623	0.044
6.20	1.704	0.008	-29.838	0.056	21.804	0.029	51.34	4.629	0.012	-158.474	0.045	-211.435	0.070
6.71	1.126	0.008	-27.820	0.011	22.272	0.009	52.34	3.004	0.011	-135.752	0.031	-215.029	0.013
7.98	0.636	0.008	-36.420	0.042	21.617	0.024	54.76	0.315	0.014	-167.874	0.022	-206.543	0.019
9.93	1.902	0.008	5.509	0.016	22.362	0.014	55.31	22.291	0.025	-144.238	0.060	-216.010	0.142
11.39	0.358	0.008	9.311	0.016	10.988	0.020	55.61	0.595	0.017	-141.600	0.037	-216.697	0.196
							55.70	1.347	0.016	-137.836	0.059	-215.194	0.012
							55.94	1.398	0.017	-166.764	0.027	-208.344	0.015
							56.51	1.092	0.010	-140.474	0.022	-215.353	0.015
							57.15	0.255	0.012	-168.077	0.009	-205.775	0.075
							57.71	3.272	0.024	-147.948	0.025	-215.954	0.007
							58.38	65.292	0.025	-163.341	0.025	-210.903	0.006
							58.86	1.089	0.025	-167.834	0.400	-206.499	0.315
							59.96	0.190	0.010	-185.803	0.020	-177.787	0.003
							60.30	7.218	0.014	-168.010	0.005	-205.339	0.011
							60.51	0.398	0.012	-146.040	0.009	-215.964	0.012
							60.62	1.412	0.012	-183.719	0.017	-193.356	0.006
							61.33	2.252	0.014	-141.725	0.017	-216.260	0.039
							61.56	1.366	0.014	-183.073	0.005	-195.755	0.004
							61.73	7.104	0.014	-143.810	0.012	-215.744	0.012
							63.79	4.307	0.012	-175.093	0.011	-199.731	0.029
							64.22	1.780	0.012	-170.420	0.017	-208.431	0.013
							64.24	5.242	0.012	-152.787	0.173	-213.286	0.051
							65.07	0.523	0.011	-151.155	0.043	-213.977	0.084
							65.07	0.264	0.011	-167.891	0.009	-205.154	0.011
							65.65	4.106	0.014	-183.197	0.035	-192.793	0.090
							65.84	4.726	0.014	-146.895	0.011	-214.922	0.043
							67.10	68.043	0.026	-182.992	0.052	-193.416	0.079
							68.01	3.221	0.026	-150.133	0.020	-213.702	0.013
							68.75	2.163	0.010	-148.472	0.033	-214.135	0.103
							71.67	0.289	0.008	-181.106	0.383	-195.699	0.081
							73.68	0.306	0.008	-180.275	0.041	-195.677	0.011
							74.22	0.400	0.008	-155.831	0.030	-209.769	0.019

TABLE 2

MASER FEATURES IN EPOCH 2 (2006 MAY 31). POSITIONS ARE RELATIVE TO THE FEATURE WITH POSITION (0,0) (IN BOLDFACE).

Blueshifted Masers							Redshifted Masers						
$v_{LSR}$ km/s	$S_\nu$ Jy/beam	$\sigma_{S_\nu}$ Jy/beam	$\Delta RA$ mas	$\sigma_{RA}$ mas	$\Delta DEC$ mas	$\sigma_{DEC}$ mas	$v_{LSR}$ km/s	$S_\nu$ Jy/beam	$\sigma_{S_\nu}$ Jy/beam	$\Delta RA$ mas	$\sigma_{RA}$ mas	$\Delta DEC$ mas	$\sigma_{DEC}$ mas
-53.27	0.287	0.016	-72.900	0.005	-58.278	0.041	37.66	0.611	0.010	-183.179	0.007	-206.927	0.003
-44.68	2.124	0.018	-72.083	0.111	-58.181	0.067	39.49	1.106	0.041	-179.300	0.017	-203.316	0.005
-34.90	2.538	0.018	-71.480	0.012	-58.045	0.008	39.57	0.358	0.017	-191.745	0.043	-194.892	0.026
-29.69	0.481	0.009	-74.157	0.005	-57.590	0.004	39.59	1.044	0.041	-179.791	0.035	-205.364	0.409
-17.93	0.308	0.008	-0.009	0.014	8.000	0.011	39.59	1.744	0.041	-182.769	0.030	-206.719	0.038
-16.06	0.574	0.011	-70.295	0.013	-58.129	0.011	39.63	2.110	0.405	-177.445	0.029	-213.267	0.019
<b>-15.94</b>	<b>2.441</b>	<b>0.011</b>	<b>0.000</b>	<b>0.012</b>	<b>0.000</b>	<b>0.018</b>	39.63	27.595	0.040	-180.170	0.008	-210.045	0.016
-8.18	0.762	0.008	6.199	0.003	11.315	0.004	39.66	1.736	0.041	-187.803	0.029	-192.371	0.053
-7.05	0.411	0.008	-6.247	0.025	17.375	0.010	39.83	1.065	0.043	-175.564	0.041	-214.059	0.091
-2.75	3.761	0.025	-24.490	0.061	19.822	0.124	40.36	10.918	0.043	-178.400	0.147	-211.032	0.237
-2.40	0.562	0.013	7.966	0.026	5.293	0.032	42.71	1.455	0.032	-181.794	0.064	-207.896	0.059
-2.07	1.541	0.025	-6.409	0.011	17.754	0.029	44.21	0.799	0.011	-141.922	0.116	-224.247	0.089
-1.79	2.538	0.020	-9.064	0.200	20.002	0.075	46.21	0.868	0.012	-170.364	0.005	-216.287	0.008
-0.57	1.429	0.015	-7.550	0.007	18.766	0.006	47.30	1.107	0.014	-140.195	0.004	-224.090	0.009
0.04	0.461	0.012	9.036	0.016	19.963	0.017	48.33	0.553	0.011	-175.995	0.031	-212.470	0.110
0.42	1.904	0.016	-33.355	0.114	20.650	0.017	49.81	0.658	0.013	-139.338	0.003	-223.616	0.004
1.48	0.810	0.010	6.161	0.125	12.045	0.035	49.89	1.039	0.012	-174.813	0.037	-213.856	0.062
3.61	1.680	0.015	-23.813	0.010	21.549	0.009	51.55	0.594	0.012	-172.694	0.022	-216.830	0.019
4.49	0.525	0.012	-38.643	0.027	21.157	0.049	51.69	0.390	0.012	-139.226	0.079	-223.407	0.028
5.46	3.033	0.022	6.980	0.068	11.041	0.151	51.69	0.569	0.012	-196.323	0.013	-197.690	0.014
6.52	1.812	0.016	-24.885	0.022	21.754	0.029	53.88	0.534	0.010	-148.819	0.042	-225.731	0.159
7.02	1.485	0.016	-29.909	0.005	21.719	0.009	55.79	0.544	0.013	-126.853	0.027	-233.320	0.008
9.35	0.516	0.009	-37.431	0.010	21.424	0.013	57.41	0.871	0.016	-168.475	0.037	-219.583	0.012
							58.91	8.976	0.038	-173.337	0.007	-214.489	0.006
							60.82	2.909	0.052	-158.830	0.005	-221.978	0.064
							63.20	8.535	0.039	-148.011	0.013	-224.128	0.015
							64.13	0.418	0.016	-189.618	0.033	-202.385	0.005
							65.27	4.154	0.031	-150.254	0.024	-224.042	0.024
							65.77	1.353	0.026	-151.707	0.010	-223.699	0.015
							66.77	1.214	0.015	-189.064	0.056	-201.638	0.064
							67.52	0.546	0.012	-150.918	0.081	-223.606	0.020
							68.50	0.526	0.010	-158.452	0.004	-221.553	0.008
							70.42	2.363	0.022	-188.246	0.136	-202.452	0.075
							70.94	0.763	0.022	-155.552	0.009	-221.343	0.014
							72.37	0.983	0.013	-187.238	0.007	-204.143	0.025
							76.14	0.648	0.010	-160.555	0.006	-217.938	0.012
							78.04	1.391	0.015	-172.903	0.009	-208.518	0.014